Low Supersonic Flow over Hemisphere-Cylinder at Incidence

Tsuying Hsieh*
ARO, Inc., Arnold Engineering Development Center, Arnold Air Force Station, Tenn.

A wind-tunnel investigation was conducted of the flow about a hemisphere-cylinder at incidence up to 19 deg in the low supersonic Mach number range from 1.1 to 1.5. Shadowgraphs, surface pressures, and oil flow pictures showing the separation patterns and limiting streamlines were obtained through the Mach number range. Surface pressure data were compared to inviscid calculations for the nonseparated regions for $M_\infty \geq 1.2$. Two separation regions, the nose separation bubble and the crossflow separation zone, were found to exist simultaneously. A concentrated vortex pair was found standing on the leeside of the forebody, and the mechanism for its appearance is discussed. The distribution of normal-force, total normal-force, and axial-force coefficients and center of pressure are presented and compared with available data and a simple theoretical prediction.

Nomenclature

C_A = axial-force coefficient (forebody only), $F_A/\frac{1}{2}\rho_\infty U_\infty^2(\pi R^2)$
C_n = coefficient of local normal force per unit length
C_N = total normal-force coefficient, $F_N/\frac{1}{2}\rho_\infty U_\infty^2(\pi R^2)$
C_P = pressure coefficient, $(p-p_\infty)/\frac{1}{2}\rho_\infty U_\infty{}^2$
F_A, F_N = axial and normal force, respectively
M_∞ = Mach number
R = radius of cylinder
Re = Reynolds number per foot, $\rho_\infty U_\infty/\mu_\infty$
S_1, S_2 = primary and secondary separation points, respectively
U, V = axial and radial (or vertical) velocity components
Y, Z = radial (or vertical) and axial distance
$(Z/R)_{c.p.}$ = axial distance of center of pressure from nosetip
α = angle of attack
Δ = shock standoff distance
μ = dynamic viscosity of the fluid
ρ = density of the fluid
ϕ = circumferential angle measured from leeside plane of symmetry
ψ_s = angle of separation in the crossflow plane

Subscripts

∞ = condition at freestream

Introduction

RECENT interest in basic aerodynamics of bodies of revolution covers the range of incidence from 0 to 180 deg.[1,2] As the incidence increases beyond 20 deg, side force and yawing moment begin to develop because of the occurrence of asymmetrical vortex patterns in the leeside flowfield. In the high subsonic, transonic, and low supersonic flow regime, the magnitude of the side force sometimes can reach as large as 60% of the normal force at an incidence between 30 and 50 deg.[3,4] It has been reported in Refs. 3 and 4 that the side force and yawing moment can be reduced by increasing the bluntness of the nose. The bluntness of the nose also has the effect of increasing the incidence for the onset of asymmetrical vortex shedding.[4] Therefore, for bodies designed for large incidence, a blunt nose may be considered for the purpose of increasing lateral stability.

The present experimental investigation was undertaken to provide needed information concerning the flowfield about blunt-nose bodies of revolution at low supersonic speeds and to determine the potential enhancement of lateral stability provided by nose bluntness. Specifically, the flowfield about a hemisphere-cylinder at incidences up to 19 deg is reported. In this range of incidence, significant side force and yawing moment are not expected; therefore, a symmetrical flowfield is assumed.

As a first step toward understanding the flowfield, particularly the separation phenomena, experimental results including shadowgraphs, oil flow pictures showing the separation patterns and limiting streamlines, and surface pressure are presented and interpreted. Inviscid calculations using the results of a time-dependent solution to Euler's equation for the hemisphere nose[5] and a three-dimensional method of characteristics for the cylinder portion[6] are compared to the experimental data at $M_\infty = 1.2$ and 1.4. Of great interest is the formation of a concentrated vortex pair standing on the leeside of the forebody at $\alpha = 19$ deg, and the mechanism for its appearance is discussed. Also two separation regions, the nose separation bubble and the crossflow separation zone, are found to exist simultaneously. By integrating the surface pressure, the distribution of local normal-force coefficient, the total normal- and axial-force coefficients, and the center of pressure were determined and are presented for comparison with available data and a simple theoretical prediction. Details of the present investigation or for $M_\infty \leq 1.0$ can be found in Ref. 7.

Test Apparatus, Experimental Technique, and Test Conditions

Wind-Tunnel Facility

The experiments described herein were performed in the Arnold Engineering Development Center (AEDC) Aerodynamic Wind Tunnel (1T) (Fig. 1). This facility is a continuous-flow, nonreturn wind tunnel capable of being operated at Mach numbers from 0.2 to 1.5. The test section is 30.5 cm square and 95.3 cm long with 6% porous walls in the top and bottom and two plexiglass side walls for flow visualization. The accuracy of Mach number in the test section is ± 0.003.

Model, Support System, and Pressure Measurements

The model used in the test is a hemisphere-cylinder 2.54 cm in diam and 25.4 cm long (Fig. 1) and is made of stainless

Received Feb. 16, 1977; revision received July 15, 1977.
Index categories: Supersonic and Hypersonic Flow; Viscous Nonboundary-Layer Flows; LV/M Aerodynamics.
*Research Engineer, PWT/4T. Member AIAA.

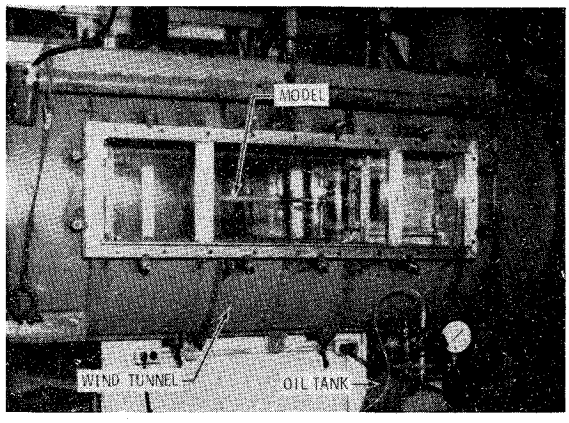

Fig. 1 Wind tunnel, model, and oil tank.

steel. Eighteen pressure orifices are located along a single plane. The model is sting-mounted with a sting diameter of 1.9 cm. An adapter is used in order to cover the incidence range up to 19 deg. The accuracy of model incidence is estimated to be ± 0.15 deg. The model can be rolled manually every 15 deg. A system of Scanivalves was used for pressure measurements, with accuracy of $\Delta C_p = \pm 0.01$.

Flow Visualization and Test Conditions

Two visualization methods were used in this experiment: shadowgraphs and oil flow pictures. The shadowgraph system is an off-axis, collimated beam, direct shadowgraph type. An air gap spark is the point light source (effective diameter = 0.102 cm), and it provides exposure of approximately 1-μsec duration. The source is positioned at the focus of a 40.6-cm-diam $f/8$ parabolic mirror. This mirror reflects light from the source in a collimated beam through the wind-tunnel test section, perpendicular to the flow, and directly onto film (28 × 35.6 cm to cover the field of interest).

The surface flow pattern is revealed by the technique of injecting oil from the pressure orifices. The pressure tubes from the model were connected into an oil tank, which was pressurized and set outside of the wind tunnel as shown in Fig. 1. Black dye was added to the oil, and the model was sprayed with a light coat of white paint to increase the contrast. Grids at intervals of 30 deg in the circumferential direction and every 1 in. in the longitudinal direction are marked on the model surface to provide readings of separation lines. Circumferential angles of $\phi = 165$, 120, 75, and 30 deg were chosen for oil injection in order to provide a comparison of surface flow pattern and separation lines. A matrix of test conditions is presented in Table 1.

Inviscid Calculation

In Ref. 5, it was found that the flowfield about a hemisphere-cylinder at zero incidence in the low supersonic Mach number range, $M_\infty \geq 1.05$, can be predicted satisfactorily by inviscid theory. Therefore, for hemisphere-cylinder at low incidence in the same Mach number range, inviscid calculation may serve as a guide in the interpretation of the experimental data. A method of inviscid calculation for low supersonic, three-dimensional flow about a hemisphere-cylinder has been reported in Ref. 6. The method has been improved since then, and computations were performed for $M_\infty = 1.2$ and 1.4 at incidence from 5 to 19 deg. A brief description of the method of calculation is given in this section, and comparison with experiments will be given in the next section.

Table 1 Test conditions[a]

M_∞	1.1	1.2	1.3	1.4	1.5
$Re \times 10^{-6}$/ft	5.4	5.4	5.3	5.3	5.0
α	A	A	A	A	A
Pressure	C	B	C	B	C
Shadowgraph	Yes	Yes	Yes	Yes	Yes
Oil flow	No	Yes	No	Yes	No

[a] A for 5, 10, 15, and 19 deg; B for $\phi = 0$, 30, 60, 75, 90, 105, 135, and 180 deg; and C for $\phi = 0$, 90, and 180 deg only.

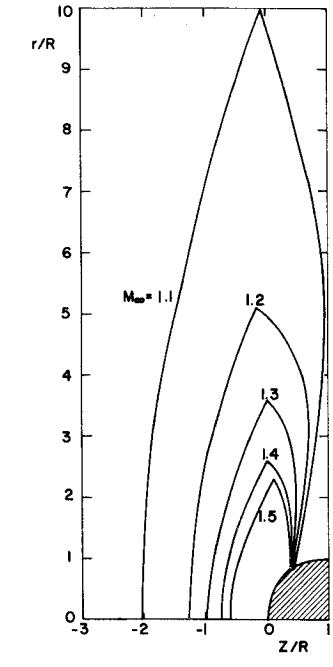

Fig. 2 Sonic line location at low supersonic Mach number for a hemisphere nose at zero incidence.

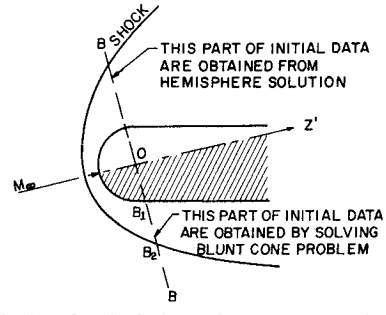

Fig. 3 Methods of calculation of low supersonic flow about a hemisphere-cylinder at incidence.

The concept of rotating the flowfield of a hemispherical-nosed blunt body by the amount of incidence of the body to provide a flowfield for the nose at incidence and the initial data for downstream three-dimensional supersonic flow computation is well known. To apply the same technique for low supersonic flow, one must be careful about the increase of subsonic region and the shock layer at the nose as shown in Fig. 2.[5] The conventional method breaks down when the subsonic and transonic regions are close to the plane at the junction of the hemisphere and the cylinder and when the incidence is large. In this case, a complete solution of the three-dimensional Euler's equations, as reported in Ref. 8, is required. Such a computation requires large computer storage and time and was not attempted in the present investigation. Thus, an approximate method of providing the flowfield to cover the subsonic and transonic region and the initial data for downstream calculation was developed.

The concept of rotating the flowfield is extended to cope with the increased subsonic and transonic region for the hemisphere nose at low supersonic Mach number. As shown in Fig. 3, plane *BB* is perpendicular to the wind direction and passing through the center of the hemisphere. It is assumed that 1) on plane *BB* the flow within the shock layer is everywhere supersonic, and 2) the body shape downstream of

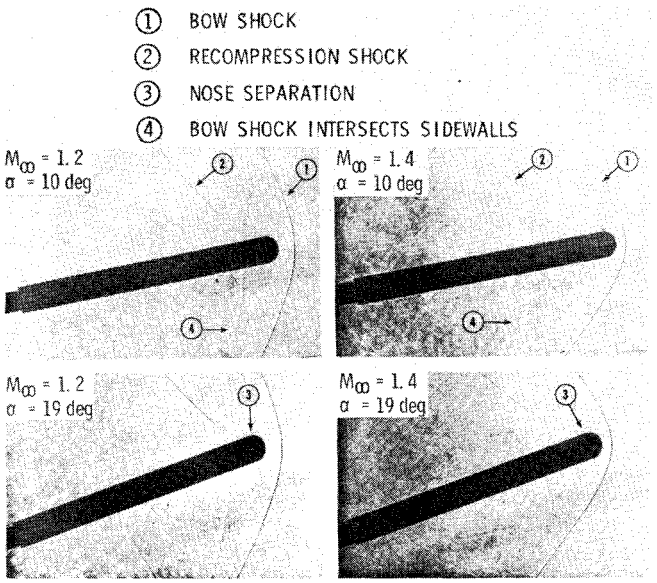

Fig. 4 Shadowgraphs for flow past hemisphere-cylinder at incidence.

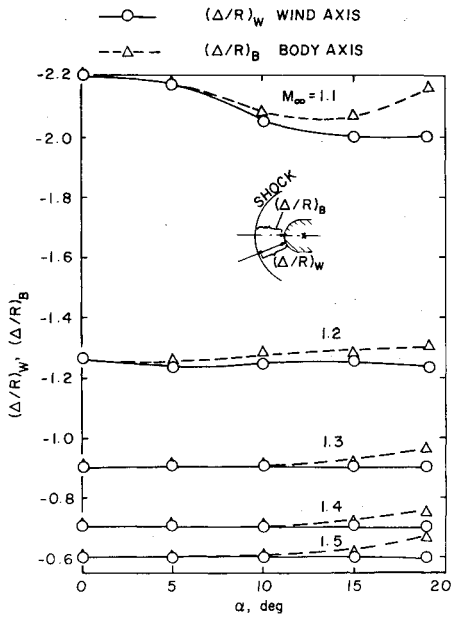

Fig. 5 Shock standoff distance about hemisphere-cylinder at incidence from shadowgraphs.

plane *BB* has no influence on the flow upstream. These assumptions will be shown to be valid for $M_\infty \geq 1.2$ from experiments in the next section. As a result, the flow upstream of plane *BB* can be calculated independently, and the three-dimensional method of characteristics may be applied to compute the downstream flowfield. In fact, the flow in the shock layer upstream of plane *BB* between $\phi = 0$ and 90 deg is essentially independent of ϕ; however, the flow between ϕ from 90 to 180 deg remains unknown and is three-dimensional in nature. As an approximation, it is assumed that the circumferential velocity component developed up to plane *BB* for $90 < \phi < 180$ deg is small and may be neglected; hence the flow on the meridian plane at a given ϕ may be approximated by an equivalent blunt cone, with the cone half-angle β given by

$$\tan\beta = \frac{\sin\alpha}{\sqrt{\cos^2\alpha + \tan^2(\pi - \phi)}} \qquad (1)$$

The flowfield of a blunt cone at low supersonic Mach number, in turn, may be computed either by the same method described in Ref. 5 or by utilizing the method of Ref. 9, as was done in Ref. 6 for $M_\infty = 1.2$. It should be noted that the calculated velocity field on the nose portion of the hemisphere-cylinder at zero incidence and $M_\infty = 1.1$ to 1.3 using the method of Refs. 5 and 9 shows good agreement within the shock layer.[10] Details of the calculation and the initial data may be found in Ref. 6.

After the initial data in plane *BB* have been obtained for the hemisphere-cylinder, the downstream flowfield is calculated by the three-dimensional method of characteristics. The computer program used in Ref. 11 was modified to perform the calculation.

Results and Discussion

Flowfield Around the Hemispherical Nose at Incidence

Figure 4 shows a few of the shadowgraphs of the hemisphere-cylinder at incidence for $M_\infty = 1.2$ and 1.4. A plot of the shock standoff distance at both the body axis and the wind axis obtained from the shadowgraphs is presented in Fig. 5. It is seen that for $M_\infty \geq 1.2$ the shock standoff distance in the wind axis is approximately constant for a given Mach number over the range of incidence under investigation. Shock shapes for $\alpha = 0$ to 19 deg at $M_\infty = 1.2$ and 1.5 are shown in Fig. 6. Also, in Fig. 6, the shock shapes for $\alpha > 0$ given by rotating the shock shape obtained at $\alpha = 0$ by angle of

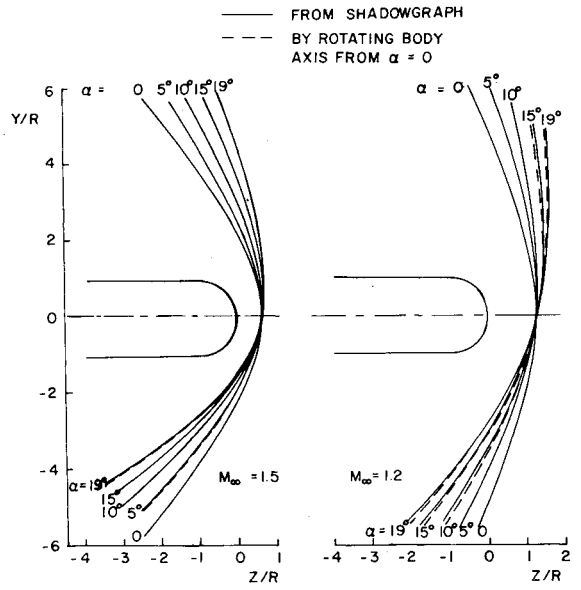

Fig. 6 Shock positions for hemisphere-cylinder at various incidences.

attack are shown by dashed lines. It is seen that the solid line and dashed line coincide very well for the case of $M_\infty = 1.5$ and differ only slightly for $M_\infty = 1.2$. These observations justify the approximations made in the flow calculation for the hemispherical nose. It should be pointed out that the flow in the nose region does not separate until 15 or 19 deg for $1.1 \leq M_\infty \leq 1.5$, as shown by the shadowgraphs[7]; hence the approximation by rotation is useful in providing initial data for inviscid computation for the downstream flowfield. A comparison of the surface pressure on the nose portion by the method of rotation with the experimental data will be given later, and the agreement is good.

Separation Characteristics

Surface flow patterns of the hemisphere-cylinder at incidence are revealed by oil flow pictures, as shown in Figs. 7a-7c. Figure 7a shows the different features of separation, and Figs. 7b and 7c show various cases. Important characteristics about the separated flow can be observed from the oil flow

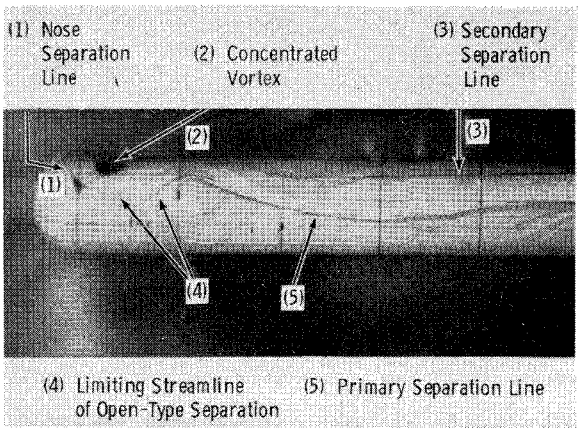

a) Various features

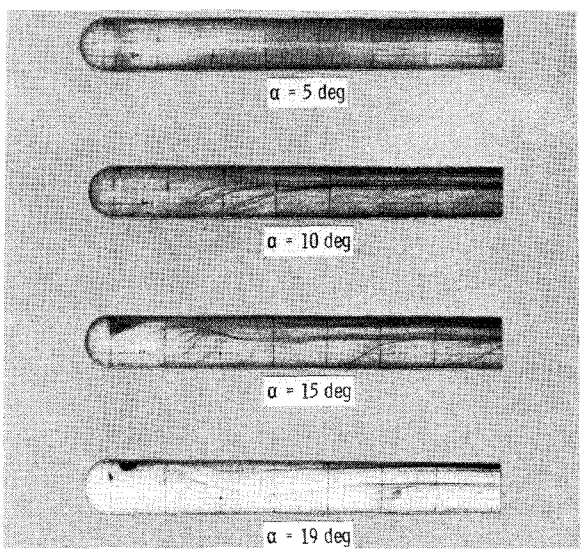

b) At $M_\infty = 1.2$

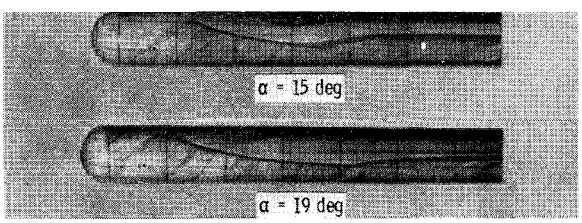

c) at $M_\infty = 1.4$

Fig. 7 Oil flow pictures showing the surface flow pattern about a hemisphere-cylinder.

pictures in conjunction with the shadowgraphs, as described below.

Regions of Separation I and II

As sketched in Fig. 8, the region of separation I is identified as the crossflow separation zone caused by the crossflow pressure gradient, a direct consequence of incidence. As a result, a pair of leeside vortex sheets appears. The region of separation II is identified as the leeside nose separation bubble caused by the meridional pressure gradient, a consequence of the bluntness of the nose, the incidence, and the freestream Mach number. (Similar nose separation also can occur at $\alpha = 0$ at transonic Mach numbers.[7]) As seen from Fig. 7b, the nose separation is not present for $\alpha \leq 10$ deg. At $\alpha = 15$ deg, there is a small separation bubble with flow reattachment. (The surface pressure there still compares favorably with the inviscid calculation, as will be shown later.) At $\alpha = 19$ deg, the nose separation bubble can be identified easily in both Figs. 4 and 7b. The role of Mach number on the nose separation can

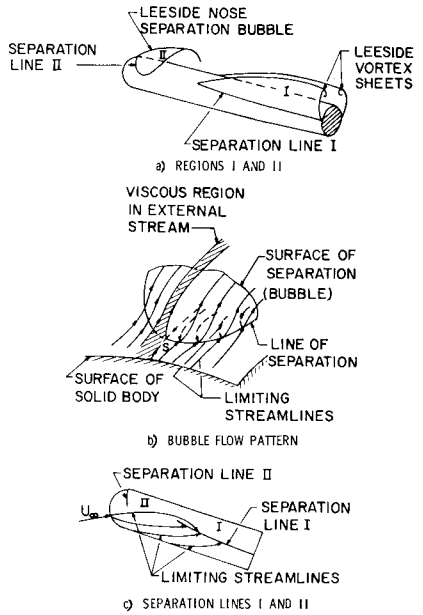

Fig. 8 Description of separation regions I and II.

be observed by comparing Figs. 7b and 7c at $\alpha = 15$ and 19 deg. It is clear that the size of separation region II decreases as the Mach number increases.

In Ref. 12, the separation patterns of elongated body of revolution at incidence are discussed in terms of open and closed separation in great detail. A simultaneous appearance of both separation regions I and II as described herein was not mentioned in Ref. 12 and hence adds a new separation phenomenon for a blunt-nose body at incidence. It therefore can be reasoned that the appearance of both separation regions I and II is a transition from an open separation to a completely closed separation.[13]

For the nose separation bubble, the bubble-type separation concept of Maskell[14] describes the flow well. Maskell's bubble-type separation as depicted in Ref. 12 is reproduced in Fig. 8b. It is noted that inside the bubble a circumferential velocity gradient can develop on the body surface near the separation line II and cause the limiting streamline to curve in a counterclockwise direction (note: in this paper, only the flow on the left side of the plane of symmetry facing upstream is discussed) toward the separation line II. At low incidence, $\alpha \sim 15$ deg, the bubble size is small, and a closed bubble can be formed with a reattachment zone. As the incidence increases, the bubble size grows by extending downstream. When the bubble size becomes sufficiently large ($\alpha \geq 19$ deg), the downstream end of the bubble becomes detached, as shown in Fig. 8a.

Even in the presence of nose separation bubble, the open-type separation line as described by Wang[12] may occur with limiting streamlines penetrating from the windward side into the leeside separation region I. This situation is sketched in Fig. 8c and is seen clearly in the oil flow picture (Fig. 7).

Appearance of a Concentrated Vortex

As shown in Fig. 7, a circulatory flow pattern appears on the cylinder surface near the nose for $\alpha = 19$ deg. This is identified as a standing concentrated vortex. A similar concentrated vortex also appears for $M_\infty = 0.8$ and 1.0,[7] whereas a concentrated vortex on the leeside front surface also has been reported by Werle.[15] However, little understanding of such a vortex has been advanced since then. With a systematic study of the oil flow pictures, a reasonable explanation of the mechanism for the formation of the concentrated vortex can be made.

The formation of the concentrated vortex at low supersonic flow can be understood as follows. For the limiting

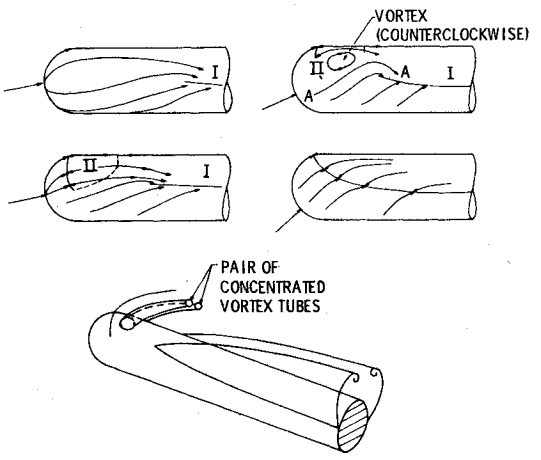

Fig. 9 Mechanism and condition for the formation of the concentrated vortex.

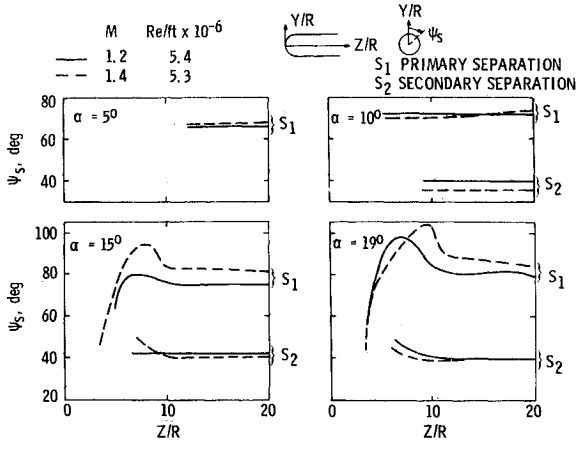

Fig. 10 Separation angle as a function of Z/R, M_∞, and α.

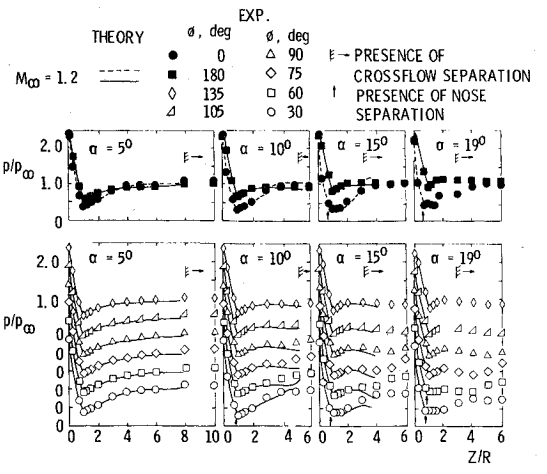

Fig. 11 Comparison of surface pressure between theory and experiments at $M_\infty = 1.2$.

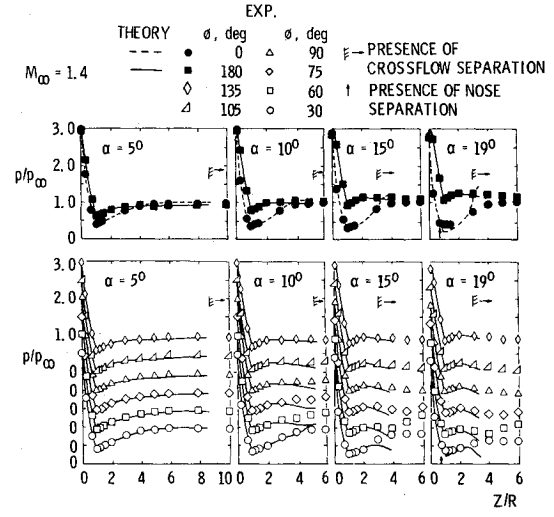

Fig. 12 Comparison of surface pressure between theory and experiments at $M_\infty = 1.4$.

streamlines at low incidence (Fig. 9a), the region of separation I is formed far downstream, and the region of separation II has not developed yet. Hence an open-type separation defined by Wang[12] prevails, as seen in Fig. 7b for $\alpha \leq 10$ deg. As the incidence increases, the region of separation II starts to develop. When the nose separation bubble is small, the flow reattaches. The limiting streamline is shown in Figs. 9b and 7b at $\alpha \sim 15$ deg. At moderate incidence (for constant Mach number), the nose separation bubble grows and becomes open; meanwhile, the open-type separation line I moves forward (see Fig. 7b at $\alpha = 19$ deg). The fluid in region II near the plane of symmetry must flow upstream, whereas that near the limiting streamlines AA (Fig. 9c) must flow downstream, and a condition is provided for the reversal of surface flow in both meridional and circumferential components. Therefore, a concentrated vortex is formed. It should be noted that the direction of the concentrated vortex is counterclockwise and therefore is consistent with the limiting streamline sketched for bubble-type separation (Fig. 8b). At still higher incidence, which is beyond the experimental range reported herein, it is believed that separation lines I and II will join together, and separation regions I and II will merge to form a closed-type separation, as sketched in Fig. 9d. Then, the concentrated vortex will disappear. Based on this reasoning, the vortex occurs only during the transition from an open separation to a completely closed separation in the presence of an open-nose separation bubble (regions II). A three-dimensional sketch of the flowfield with the presence of the concentrated vortex tubes is given in Fig. 9e. It is seen that the axis of the concentrated vortex is perpendicular to the body at the surface and is convected downstream above the body.

Secondary Separation

Also shown in the oil flow pictures of Fig. 7 is the existence of a secondary separation line. The appearance of secondary separation has been reported (Ref. 16, for example). The separation angles for the primary and secondary separation (read from the oil flow pictures) along the body axis are shown in Fig. 10. It is seen that the primary separation angle varies significantly as the Mach number increases at higher incidence, whereas the secondary separation angles are not very sensitive to changes in Mach number and angle of attack.

Surface Pressure Distribution

As discussed earlier, at small incidence the flow in the fore portion of the hemisphere-cylinder is not separated; hence an inviscid calculation has been performed for $M_\infty = 1.2$[6] and 1.4. A modification of the three-dimensional method-of-characteristics computer program[11] was made to obtain results to the location where crossflow separation is known to occur. A plot of the theoretical and experimental results is shown in Figs. 11 and 12 at various incidences for $M_\infty = 1.2$ and 1.4, respectively.

It is interesting to note that the behavior of the surface pressures on the leeside and the windward side of the plane of symmetry, as predicted by the inviscid theory, differs from the general expectation that they should gradually approach each other toward the downstream end of the body. Instead, the two curves (solid and dashed) are observed first to cross over and then to approach each other gradually. The

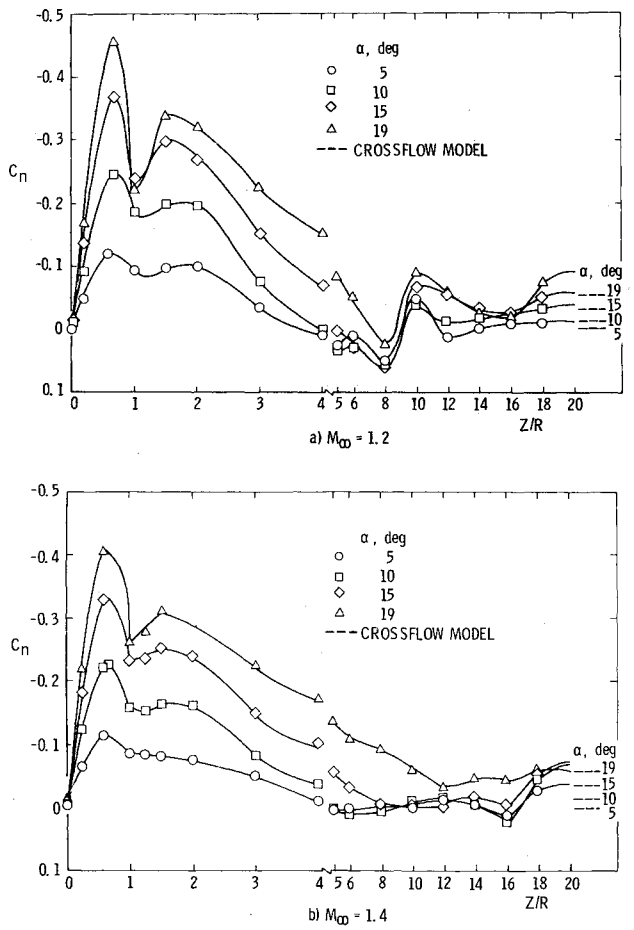

Fig. 13 Normal-force distribution over hemisphere-cylinder.

crossover character prevails for all cases computed. The crossover character is also present in the experimental data and $M_\infty = 1.2$ and 1.4 for $\alpha = 5$ deg and for $\alpha = 10$ deg to a lesser degree. Since for $\alpha = 5$ deg crossflow separation occurs far downstream, the flow over the fore portion of the body is essentially inviscid. Therefore, the theoretically predicted crossover character is indeed correct. As the incidence increases and the crossflow separation line I moves upstream (see Fig. 7 as discussed earlier), the crossover character in the real flow is lost because of viscosity, as shown by the experimental data.

Also shown in Figs. 11 and 12 are the locations where the crossflow separation and the nose separation start as estimated from the oil flow pictures and shadowgraphs. It is seen that the agreement between theory and experiment is good in the portion where the flow is not separated. It is also interesting to observe that, at $\alpha = 15$ deg, the comparison between the theory and experiments near the leeside of the nose is good for $M_\infty = 1.4$, whereas that for $M_\infty = 1.2$ is not as good, an indication of flow separation there. However, the reasonably good agreement of pressure with the separation bubble present is an indication that the separation bubble is thin and does not affect the inviscid flowfield greatly. The preceding observation also is consistent with the earlier statement that, as the freestream Mach number increases, the nose separation is suppressed. From the results of Figs. 11 and 12, it is seen that, in the low supersonic flow regime, the inviscid calculation for the hemisphere-cylinder is good for low incidence ($\alpha \lesssim 15$ deg) and from the nose down to the location where leeside crossflow separation occurs.

Aerodynamic Coefficients

The aerodynamic coefficients and the center of pressure were obtained by integrating the surface pressure. The normal-force distribution over the body length is shown in Fig. 13. Also shown in Fig. 13 is the normal force obtained by the method of crossflow drag coefficient of Ref. 1. The agreement between the experimental data and the prediction method of Ref. 1 is fairly good far downstream from the nose.

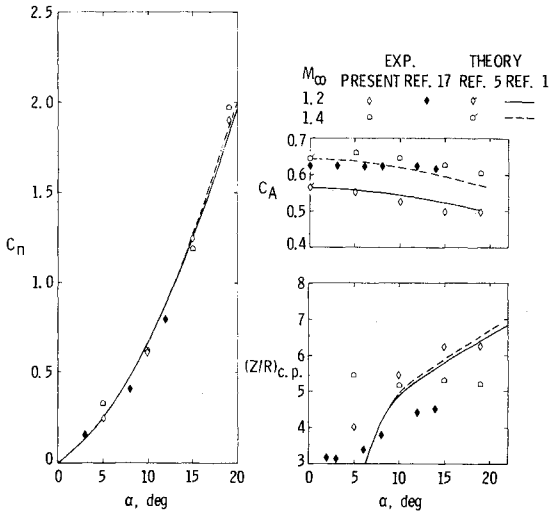

Fig. 14 Total normal-force and axial-force coefficients and center of pressure as a function of incidence.

The integrated total normal-force coefficients, axial-force coefficients, and center of pressure from the present experiments are shown in Fig. 14 (inviscid calculation[6] only performed to the point where crossflow was known to occur, and hence not used to calculate aerodynamic coefficients). The data of Ref. 17 (fineness ratio 9) using balances for force and moment measurements (for $M_\infty = 1.2$ only) also are presented for comparison. The comparison for C_N among the data is satisfactory. The crossflow model of Ref. 1 predicts C_N well. The comparison of C_A shows some difference between the present data and the referenced experiments. This is expected because the present data do not include surface frictional drag. (Note: If a frictional resistance coefficient $C_f = 0.00025$ is assumed, the surface frictional drag in the present experiment is estimated to be about 0.1, which is about the magnitude of difference in C_A between the solid and open data in Fig. 14.) Theoretical values of C_A at $\alpha = 0$ are obtained from an inviscid calculation[5] and are seen to agree very well with the present experimental data. The $\cos^2\alpha$ variation of axial force as given by the crossflow drag model[1] is fairly good in the incidence range under investigation. The comparison of center of pressure $(Z/R)_{c.p.}$ shows that the present data locate the center of pressure about 1 radius downstream of the location reported in Ref. 17. This is because of the difference in fineness ratio, as expected. The crossflow model gives $(Z/R)_{c.p.} = 1.5$ at $\alpha = 5$ deg (out of the figure); hence the theory appears to give a wrong trend for the center of pressure as α approaches 0.

Conclusions

1) For $M_\infty \geq 1.2$, it is shown that the flowfield on the hemisphere portion of a hemisphere-cylinder at incidence may be approximated by rotating the zero-incidence flowfield by the amount of incidence.

2) Two separation regions, namely, the nose separation bubble and the crossflow separation zone enclosed by leeside separation sheets, are shown to exist simultaneously at intermediate incidence. The size of the nose separation bubble decreases as the freestream Mach number increases. The downstream side of the nose separation first is reattached at small incidence and becomes detached as the incidence increases.

3) A concentrated vortex was found for incidence of 19 deg behind the nose separation line at Mach numbers 1.2 and 1.4.

Therefore, a circulatory surface flow pattern (in counterclockwise direction on the left side of the plane of symmetry when facing upstream) prevails on the leeside of the forebody near the nose. The concentrated vortex is perpendicular to the body at the surface and convected downstream above the body.

4) For $M_\infty \geq 1.2$, the inviscid computation by the approximate method described in this paper for the surface pressure is satisfactory for incidence up to 15 deg, above which nose separation occurs, from the nose down to the location where the crossflow separation is known to occur. At low incidence, the surface pressure curves for the leeside and windward side plane of symmetry are shown first to cross over and then to approach each other further downstream.

5) The crossflow drag theory of Ref. 1 predicts the total normal force well. The variation of axial force as a function of cosine square of the incidence is good for the range of incidence under investigation. The comparison of center of pressure between theory and experiments is fair but becomes poor as the incidence approaches zero.

Acknowledgments

The assistance of G. Lewis and W.C. Armstrong in performing the inviscid calculation is gratefully acknowledged. The research reported herein was conducted by the Arnold Engineering Development Center (AEDC), Air Force Systems Command (AFSC), and sponsored by the Air Force Flight Dynamics Laboratory, Wright-Patterson Air Force Base, Ohio. Research results were obtained by personnel of ARO, Inc., contract operator at AEDC. Material in this paper was presented partially in Refs. 6 and 7.

References

[1] Jorgensen, L.H., "Prediction of Static Aerodynamic Characteristics for Space-Shuttle-Like and Other Bodies at Angles of Attack from 0° to 180°," NASA TN D-6996, Jan. 1973.

[2] Fleeman, E.L. and Nelson, R.C., "Aerodynamic Forces and Moments on a Slender Body with a Jet Plume for Angles of Attack Up to 180 Degrees," AIAA Paper 74-110, 12th Aerospace Sciences Meeting, Jan. 30-Feb. 1, 1974.

[3] Pick, G.S., "Side Forces on Ogive-Cylinder Bodies at High Angles of Attack in Transonic Flow," *Journal of Spacecraft and Rockets,* Vol. 9, June 1972, pp. 389-390.

[4] Keener, E.R. and Chapman, G.T., "Onset of Aerodynamic Side Forces at Zero Sideslip on Symmetric Forebodies at High Angles of Attack," AIAA Paper 74-770, Mechanics and Control of Flight Conference, Aug. 5-9, 1974.

[5] Hsieh, T., "Hemisphere-Cylinder in Low Supersonic Flow," *AIAA Journal,* Vol. 13, Dec. 1975, pp. 1551-1552.

[6] Hsieh, T., "Low Supersonic, Three-Dimensional Flow About A Hemisphere-Cylinder," AIAA Paper 75-836, 8th Fluid and Plasma Dynamic Conference, June 16-18, 1975.

[7] Hsieh, T., "An Investigation of Separated Flow about a Hemisphere-Cylinder at 0- to 19-deg Incidence in the Mach Number Range from 0.6 to 1.5," Arnold Engineering Development Center, AEDC-TR-76-112, July 1976; also AIAA Paper 77-179, 15th Aerospace Sciences Meeting, Jan. 24-26, 1977.

[8] Morretti, G. and Bleich, G., "Three-Dimensional Flow Around Blunt Bodies," *AIAA Journal,* Vol. 5, Sept. 1967, pp. 1557-1562.

[9] South, J.C. Jr. and Jameson, A., "Relaxation Solutions for Inviscid Axisymmetric Transonic Flow over Blunt or Pointed Bodies," *Proceedings of AIAA Computational Fluid Dynamics Conference,* July 19-20, 1973.

[10] Hsieh, T., "Analysis of Velocity Measurements about a Hemisphere-Cylinder Using a Laser Velocimeter," *Journal of Spacecraft and Rockets,* Vol. 14, May 1977, pp. 280-283.

[11] Armstrong, W.C. and Bauer, R.C., "Analysis of Three-Dimensional Inviscid Supersonic Flow Between a Body and an Outer Wall," Arnold Engineering Development Center, AEDC-TR-76-103, 1976.

[12] Wang, K.C., "Separation Patterns of Boundary Layer over an Inclined Body of Revolution," *AIAA Journal,* Vol. 10, Aug. 1972, pp. 1044-1050.

[13] Hsieh, T. and Wang, K.C., "Concentrated Vortex on the Nose of an Inclined Body of Revolution," *AIAA Journal,* Vol. 14, May 1976, pp. 698-700.

[14] Maskell, E.C., "Flow Separation in Three Dimensions," Royal Aircraft Establishment, Bedford, England, RAE Rept. Aero 2565, Nov. 1955.

[15] Werle, H., "Separation on Axisymmetrical Bodies at Low Speed," *La Recherche Aeronautique,* No. 90, Sept.-Oct. 1962, pp. 3-14.

[16] Rainbird, W.J., Crabbe, R.S., Peake, D.J., and Meyer, R.F., "Some Examples of Separation in Three-Dimensional Flows," *Canadian Aeronautic and Space Journal,* Vol. 12, Oct. 1966, pp. 409-423.

[17] Anderson, C.F. and Henson, J.R., "Aerodynamic Characteristics of Several Bluff Bodies of Revolution at Mach Numbers from 0.6 to 1.5," Arnold Engineering Development Center, AEDC-TR-71-82, (AD885911), July 1971.